Textures and Microstructures, Vol. 34, pp. 119–146
Reprints available directly from the publisher
Photocopying permitted by license only

THE MICROSTRUCTURAL CHARACTERIZATION OF ELECTROGALVANIZED ZINC–IRON AND ZINC–NICKEL COATINGS

H. PARK* and J.A. SZPUNAR

Department of Metallurgical Engineering, McGill University, 3610 University Street, Montreal, PQ, H3A 2B2, Canada

(Received 8 October 1999)

In this study, the development of the microstructure of zinc–iron and zinc–nickel coatings on steel sheet electrodeposited at various deposition conditions, is analyzed. The evolution of the coating microstructure – texture, surface morphology, crystallographic lattice, microstress, alloy composition and phase of coatings – is investigated at different current densities and deposition times. The microstructure of zinc alloy coatings varies significantly with the change of deposition parameters. The present study proposes that the transformation of texture during the alloy codeposition is closely related to the morphological characteristics of the coating surface and the change of alloy and phase composition of the deposit. Anomalous codeposition behavior, is considered responsible for the change or transformation of the microstructure of coatings. The texture of zinc–iron coatings changes from the combined texture of the basal fiber and non-fiber pyramidal component to the pyramidal fiber texture with the current density increase. In the case of zinc–nickel coatings, the intensity of the {101} texture of γ phase increases with increasing nickel content, while the intensity of the {100} texture decreases. A correlation between the texture, morphology and alloy content in the deposits is discussed.

Keywords: Texture; Morphology; Zinc–iron; Zinc–nickel; Electrogalvanized coating; Anomalous codeposition

INTRODUCTION

Zinc alloy coatings have been widely used by the automotive industry because of some advantages which zinc coatings cannot provide.

* Corresponding author.

Chen and Snyder (1990) reported that by alloying zinc with other elements, a thinner, less anodic coating is formed which can provide similar corrosion resistance to pure zinc coatings. The other advantages of zinc alloy coatings are improved formability and weldability. It has been reported that zinc–iron and zinc–nickel alloy coatings not only provide excellent corrosion resistance but also exhibit improved mechanical properties compared to zinc coatings. The microstructure of zinc alloy coatings is closely related to the alloy content and phase composition of the deposit. The phase composition of electrodeposited zinc alloy coatings is found to be different from that of thermally prepared zinc alloy coatings (Lin, 1992). This is attributed to the formation of a metastable or non-equilibrium phase upon electrodeposition.

It has been known that two or more metals can be co-deposited on a steel substrate under proper conditions. Since alloy electrodeposition is more complicated than the deposition of pure metal, two conditions are critical for the alloy deposition: (1) at least one of the metals must be capable of being deposited independently, and (2) their deposition potentials must have similar values. The second condition is essential in order to avoid preferential deposition of a more noble metal which has a greater deposition driving force (Brenner, 1963; Lowenheim, 1978). The electrodeposition of zinc–iron and zinc–nickel coatings provide various textural and morphological characteristics based on the different alloy composition of the deposits. The alloy composition of the coatings is not only governed by the bath composition but also by the applied current density, because the current density is responsible for the anomalous codeposition behavior. Experimental results have been found regarding the anomalous codeposition of zinc–iron coatings (Johnson and Vrable, 1984; Irie, 1990; Lin, 1992). Irie (1990) observed that the iron content increases rapidly with the increasing current density during zinc–iron codeposition. Lin (1992) found that the iron content continuously increases from about 3% to 14%, while the current density increases from 450 to 1080 mA/cm^2. Moreover, the crystallographic structure and phase composition of the coatings are directly influenced by the anomalous codeposition behavior. This paper demonstrates how the texture and morphology of coatings evolve at various deposition conditions in conjunction with compositional change during the alloy codeposition.

EXPERIMENTAL PROCEDURE

A detailed sample preparation procedure was described by Park and Szpunar (1997). For the zinc–iron coatings, the electrodeposition was performed in a bath composed of ferrous sulfate, zinc sulfate, ammonium sulfate, potassium chloride and citric acid in concentrations of 158, 107, 100, 10 and 0.4 g/l, respectively. The bath temperature was kept constant at 50°C ± 2°C. In the case of zinc–nickel coatings, the bath is composed of zinc sulfate, nickel chloride and ammonium chloride in concentrations of 143, 366 and 30 g/l. The surface morphology of the coatings was examined by atomic force microscopy (AFM) and SEM. The AFM, a Digital Instrument Nanoscope III, was operated in the contact mode using a silicon nitride cantilever. The change of interplanar spacings and c/a ratio were calculated from the shifted angles of each diffraction peak measured using a Rigaku X-ray diffractometer. The full width half maxima (FWHM) of peaks were measured to estimate any change in the internal stress of the specimens. The texture of the specimens was analyzed using a Siemens X-ray diffractometer. The diffractometer was operated using Cu-Kα radiation at an accelerating voltage of 40 kV and a current of 40 mA. Pole figures were measured using the reflection technique up to 80° maximum tilt of the specimen in 5° polar and angular intervals.

EXPERIMENTAL RESULTS

The Surface Morphology of Zinc Alloy Coatings

The Influence of Current Density (Zinc–Iron Coatings)

The zinc–iron coatings were electrodeposited at different current densities ranging from 50 to 500 mA/cm^2. The pH of the electrolyte was kept around 3–8 and the bath temperature was kept at 50°C. The electrodeposition time was adjusted to produce coatings with a thickness of 5 μm. The morphology of the coatings significantly changes with the change of applied current density as is shown in Fig. 1. The coating deposited at a current density of 50 mA/cm^2 exhibits the morphology of hexagonal platelets and ridges. The hexagonal platelets

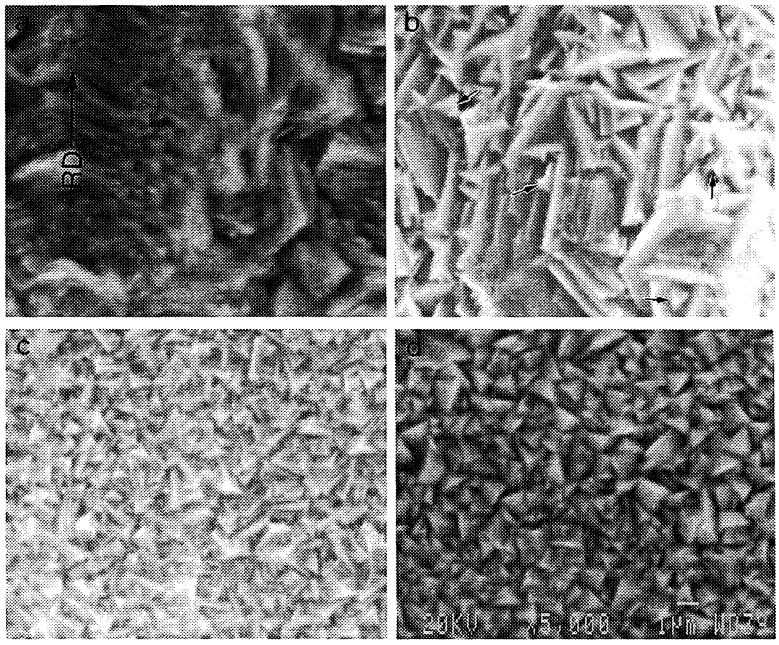

FIGURE 1 The SEM images exhibit morphological evolution of zinc–iron electrodeposited coatings at different current density: (a) 50, (b) 100, (c) 200, (d) 300 mA/cm^2; the morphology of coatings continuously changes from hexagonal platelets and ridges to triangular-based pyramids with current density increase.

are randomly distributed, while the ridges are aligned parallel to the rolling direction of the steel substrate (arrow marked in Fig. 1(a)). The average size of the hexagonal platelets is 3–6 μm. As the applied current density increases, the hexagonal platelets and ridges gradually disappear while the pyramidal morphology becomes predominant. Figure 1(b) shows that the coating deposited at 100 mA/cm^2 exhibits a mixed morphology of hexagonal ridges and pyramidal grains. These pyramidal grains are about 1 μm in size, and evolve from the boundaries between the ridges as indicated by the arrows in Fig. 1(b). As the applied current density increases to 200 mA/cm^2, the coating surface is completely covered with fine pyramidal grains, whereas no hexagonal platelets or ridges are found (Fig. 1(c)). The pyramidal grains continue to grow as the current density increases to 300 mA/cm^2 (Fig. 1(d)). Figure 1(d) shows well-developed triangular-based pyramids about the

size of 1–3 μm. The pyramidal grains are randomly distributed over the surface. A further increase in current density up to 500 mA/cm^2 does not change the morphology of the triangular-based pyramids.

Detailed observations of surface morphology were carried out by AFM. An example of the triangular-based pyramid morphology obtained at 500 mA/cm^2 is shown in Fig. 2. The AFM images show that each of the triangular-based pyramidal grains represent part of the hexagonal columnar crystal which is tilted from the substrate surface. A good agreement is found with the results of the AFM section profile analysis. The section analysis was conducted along the two $\{10\bar{1}0\}$ prismatic planes. The profile analysis shows that the angle between each $\{10\bar{1}0\}$ plane is about 120° which corresponds to the hexagonal geometry. Therefore, it is evident that the morphology of triangular-based pyramids represents a part of the hexagonal columnar crystal which consists of one {0001} plane and two $\{10\bar{1}0\}$ planes.

The EPMA (Electron Probe Micro Analysis) was conducted on the zinc–iron coatings deposited at various current densities. It is found from the EPMA results that the iron content in the deposit changes as the applied current density changes (Fig. 3). As the current density increases from 50 to 300 mA/cm^2, the percentage of iron in the zinc–iron coatings increases from 1.8 to 9.8. A further increase in the current density up to 500 mA/cm^2 causes a slight increase in the percentage of iron to 10.5.

The Influence of Coating Thickness (Zinc–Iron Coatings)

The zinc–iron coatings were electrodeposited with different deposition times to produce coating thicknesses of 5, 10, 30, and 100 μm. The current density was kept constant at 300 mA/cm^2. Figure 4 exhibits the morphology of the coatings at different coating thicknesses. At a thickness of 5 μm, the coating shows typical triangular pyramidal grains. As the coating thickness increases to 10 μm, the surface morphology is dominated by large pyramidal grains with a size of 3–4 μm. A further increase in coating thickness to 30 μm causes a morphological transformation to the randomly oriented hexagonal ridges. Eventually, hexagonal columnar crystals evolve when the coating thickness reaches 100 μm. The coating deposited at the higher current density of 500 mA/cm^2 has a completely different morphology. Figure 5 shows an example

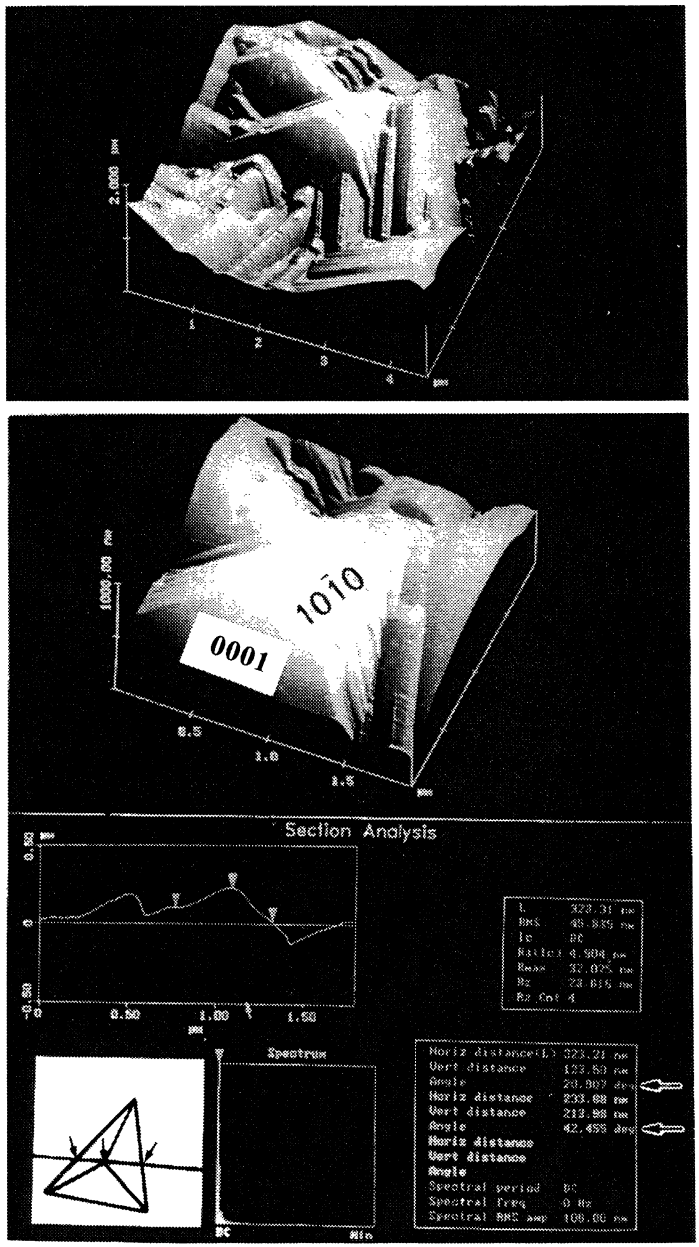

FIGURE 2 The AFM morphology and section profile analysis of triangular pyramidal morphology of zinc–iron electrodeposited coatings; the pyramid represents part of a hexagonal columnar crystal tilted from the substrate surface. Thus, one wall represents {0001} plane while the other two walls represent $\{10\bar{1}0\}$ planes. The section analysis exhibits the angle between each $\{10\bar{1}0\}$ plane is about 120° which corresponds to the hexagonal geometry.

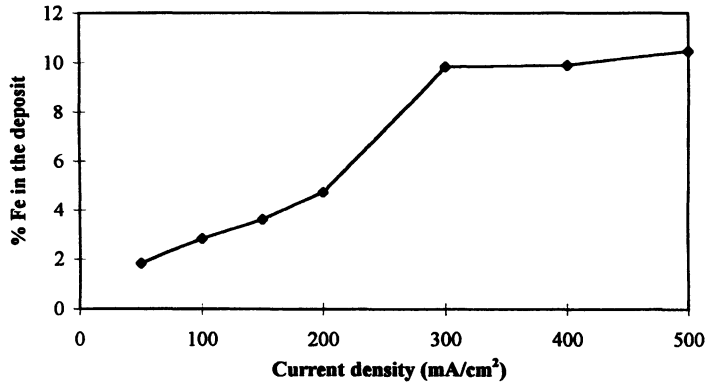

FIGURE 3 The change of iron content in the zinc–iron electrodeposited coatings at various current densities.

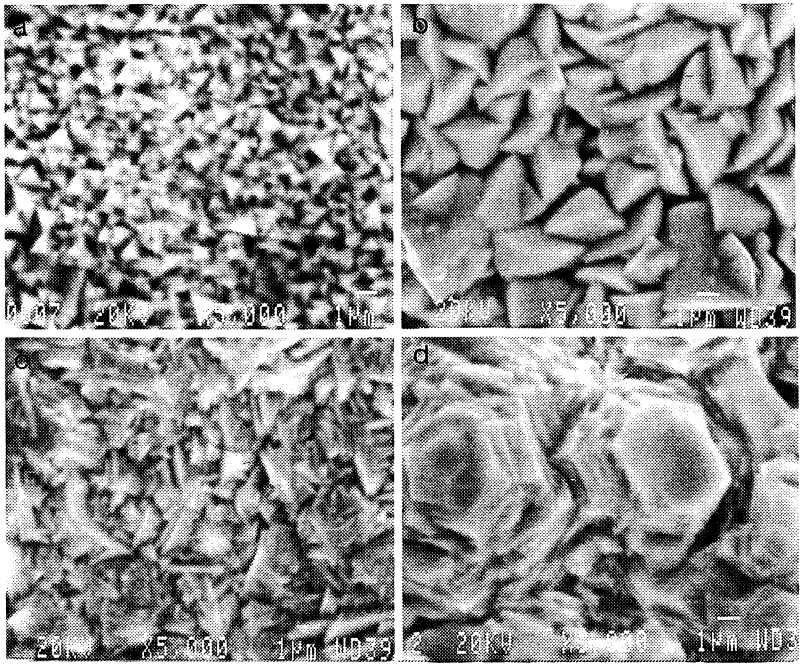

FIGURE 4 The SEM images exhibit morphological evolution of zinc–iron electrodeposited coatings at different coating thicknesses (current density at 300 mA/cm^2): (a) 5, (b) 10, (c) 30, (d) 100 μm.

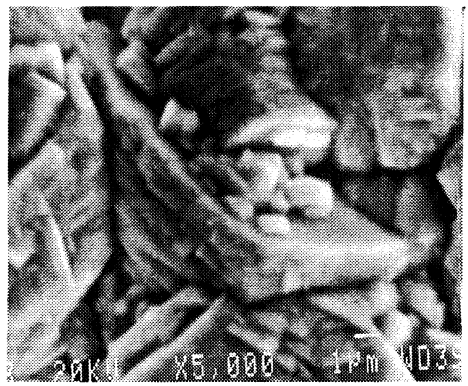

FIGURE 5 The SEM image of zinc–iron electrodeposited coating with a coating thickness of 100 μm, deposited at 500 mA/cm^2.

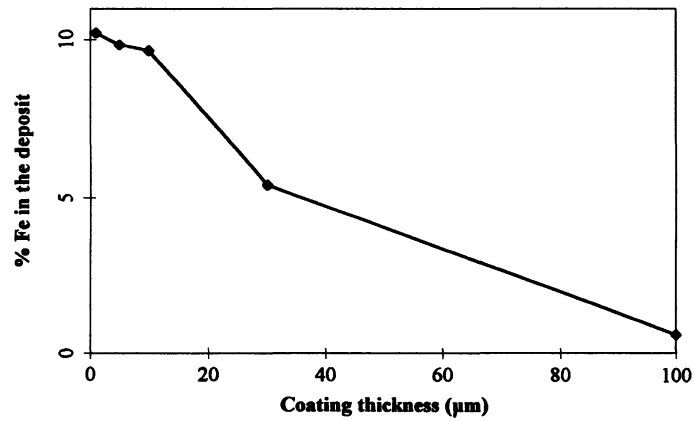

FIGURE 6 Correlation between coating thickness and percent of iron in the zinc–iron electrodeposited coatings.

of the morphology of large hexagonal ridges in the coatings having a thickness of 100 μm. The current density is usually associated with a change in alloy composition. The EPMA indicates that the alloy composition of coatings changes as the coating thickness changes (Fig. 6). In the case of coatings deposited at 300 mA/cm^2, as the coating thickness increases from 1 to 100 μm, the percentage of iron in the zinc–iron coating significantly decreases from 10.2 to 0.6.

The Influence of Current Density (Zinc–Nickel Coatings)

This section describes the influence of current density upon the coating morphology of zinc–nickel coatings. The zinc–nickel coatings were electrodeposited under different current densities ranging from 50 to 1200 mA/cm^2. The pH of the electrolyte was kept at about 2.3. The electrodeposition time was adjusted to produce a coating with a thickness of 15 μm. Figure 7 shows different coating morphologies produced at different current densities. The coating deposited at 50 mA/cm^2 shows the morphology of pyramids. As the deposition current density increases to 200 mA/cm^2, the coating morphology transforms to the nodular pyramidal grains. The size of the grains is about 1–2 μm. Additional increases of current density up to 500 mA/cm^2 does not cause any significant morphological change. Eventually, a further increase in current density to 1200 mA/cm^2 results in a completely different coating morphology. The coating surface is

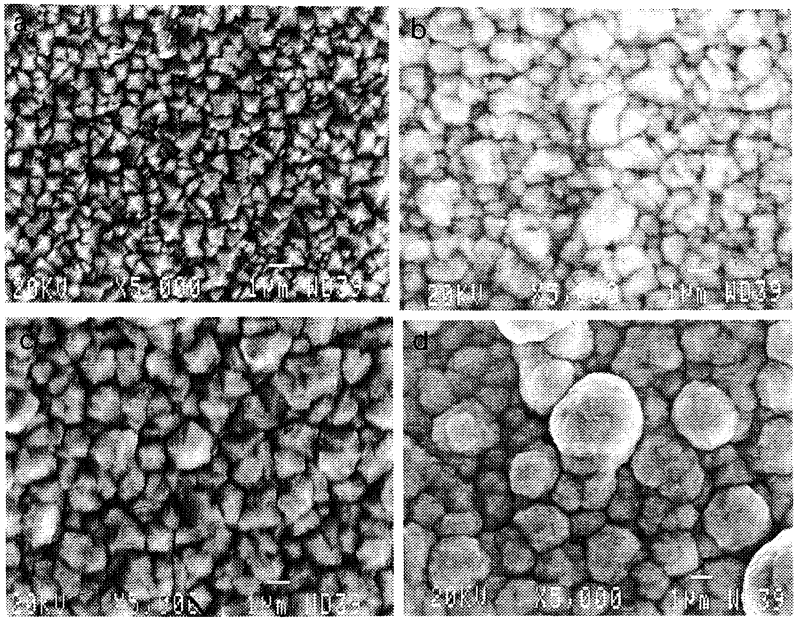

FIGURE 7 The SEM images exhibit morphological evolution of zinc–nickel electrodeposited coatings at different current density: (a) 50, (b) 200, (c) 500, (d) 1200 mA/cm^2.

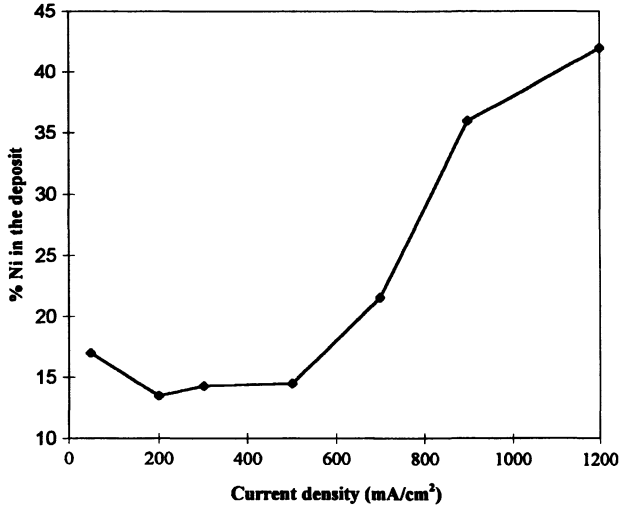

FIGURE 8 Correlation between current density and percent of nickel in the zinc–nickel electrodeposited coatings.

covered by a number of submicron sized grains conglomerated together to form the "cauliflower-like" structure.

Nickel percent was measured in the zinc–nickel coatings deposited at various current densities. As is the case in zinc–iron coatings, the nickel content of zinc–nickel coatings significantly changes as the deposition current density changes (Fig. 8). The EPMA indicates that the coatings deposited at the current density of 50 mA/cm^2 have about 17% of Ni in the deposit. As the current density increases to the range of 200–500 mA/cm^2, the nickel content in the deposit drops to 13–15%. A further increase of the current density up to 1200 mA/cm^2 results in a dramatic increase of nickel content up to 42%.

Crystallographic Structure of Coatings

The Change of the Interplanar Spacings of Zinc–Iron Coatings with Current Density

The zinc–iron coatings deposited at different current densities were analyzed using an X-ray diffractometer. Figure 9 shows various X-ray diffraction patterns of zinc–iron coatings deposited at different current

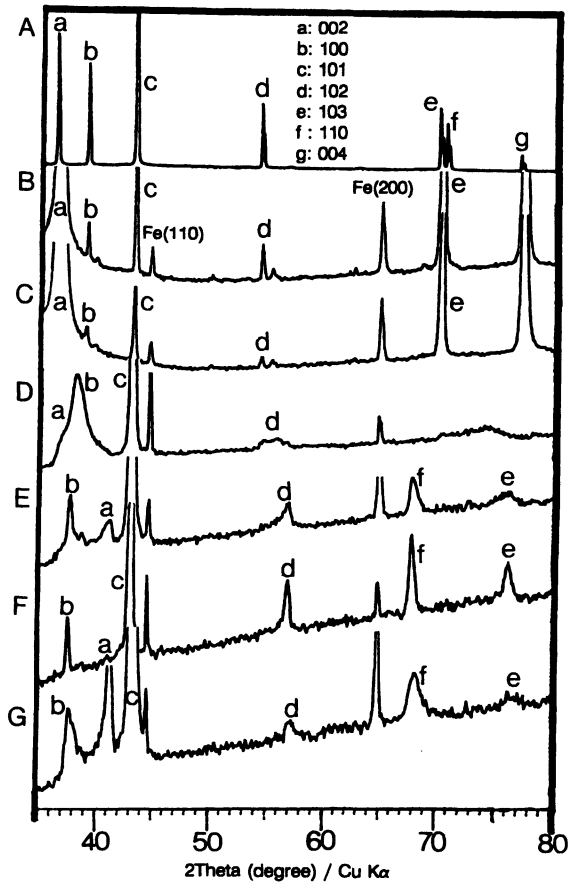

FIGURE 9 X-ray diffractometry of zinc–iron electrodeposited coatings at various current density: (a) zinc random powder, (b) 50, (c) 100, (d) 200, (e) 300, (f) 400, (g) 500 mA/cm^2; each of the peaks shift either to higher or lower 2θ angles as the current density changes.

densities ranging from 50 to 500 mA/cm^2. All the coatings have peaks which represent the η phase. It is noticeable that each of the peaks which represents a specific crystallographic plane gradually shifts either to higher or lower 2θ angles as the current density changes. The {0002} peak, for instance, is located at the lowest 2θ position for the coating deposited at 50 mA/cm^2. As the current density increases, the {0002} peak gradually shifts to a higher angle. Eventually, the {0002} peak shifts

to a higher 2θ position than the $\{10\bar{1}0\}$ peak, as the current density increases up to 500 mA/cm^2. By contrast, the $\{10\bar{1}0\}$ peak shifts to a lower 2θ value as the current density increases. Meanwhile, the $\{10\bar{1}0\}$ peak does not shift significantly with the current density increase. It is also observed that the $\{10\bar{1}2\}$ and $\{10\bar{1}3\}$ peaks shift to higher 2θ values, whereas the $\{11\bar{2}0\}$ plane shifts to a lower 2θ value as the current density increases.

Figure 10 illustrates the change of interplanar spacings of the η phase as a function of current density. As the current density increases, the interplanar spacing of {0002}, $\{10\bar{1}2\}$ and $\{10\bar{1}3\}$ planes decrease,

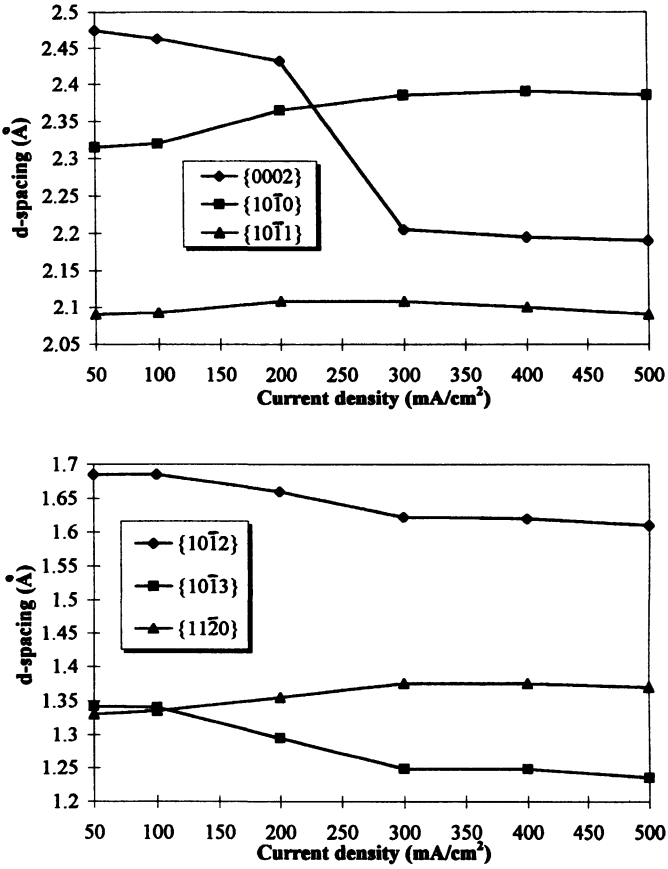

FIGURE 10 Correlation between deposition current density and interplanar spacings of zinc–iron electrodeposited coatings.

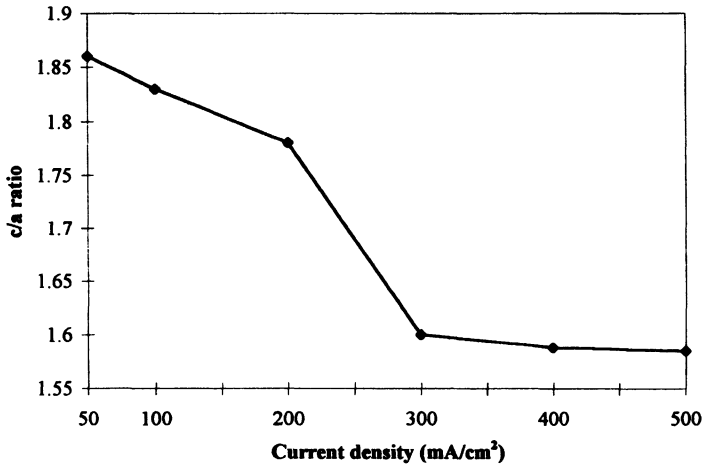

FIGURE 11 Correlation between deposition current density and c/a ratio of zinc–iron electrodeposited coatings.

whereas the interplanar spacing of $\{10\bar{1}0\}$ and $\{11\bar{2}0\}$ increase. It should be noted that the change of interplanar spacing is most significant at a current density range between 200 and 300 mA/cm^2. The c/a ratio was calculated from this X-ray diffraction data, and plotted against the current density change (Fig. 11). The coating deposited at 50 mA/cm^2 has the c/a ratio of 1.86. The c/a ratio gradually decreases as the current density increases. The coatings deposited at 100 and 200 mA/cm^2 have a c/a ratio of 1.83 and 1.78, respectively. A sudden drop of c/a to 1.6 is found at the current density range between 200 and 300 mA/cm^2. A further increase in current density from 300 to 500 mA/cm^2 does not influence the c/a ratio. As previously described above, the percentage of iron in the zinc–iron coating increases as the current density increases. Therefore, the c/a ratio and the percentage of iron in the coatings are correlated. The c/a ratio decreases as the percentage of iron increases. This result is in agreement with other experimental works (Shima *et al.*, 1986; Lin, 1992; Kondo, 1994).

The Change of the Phase Composition of Zinc–Nickel Coatings with Current Density

To determine the phase composition of zinc–nickel coatings, X-ray diffraction patterns were measured at various current densities. Unlike

the zinc–iron coatings which have a single η phase in the previous section, the zinc–nickel coatings have peaks which represent the secondary γ phase at a high current density. Figure 12 shows the X-ray diffraction peaks of electrodeposited zinc–nickel coatings at the current density range of 50–1200 mA/cm^2. Overall, the coatings have either the η peak which represents the $\{10\bar{1}0\}$ or the γ peaks which represent the {411/330} or {442/600}. There are no other peaks found which represent other planes of the η or the γ phases. The X-ray diffraction data shows that the coating deposited at 50 mA/cm^2 has two major peaks which represent the η $\{10\bar{1}0\}$ as well as the γ {442/600}. The intensity of the η peak is stronger than the γ peak. At the current density of 100 mA/cm^2, the coating also has the η $\{10\bar{1}0\}$ peak and the γ {442/600} peak.

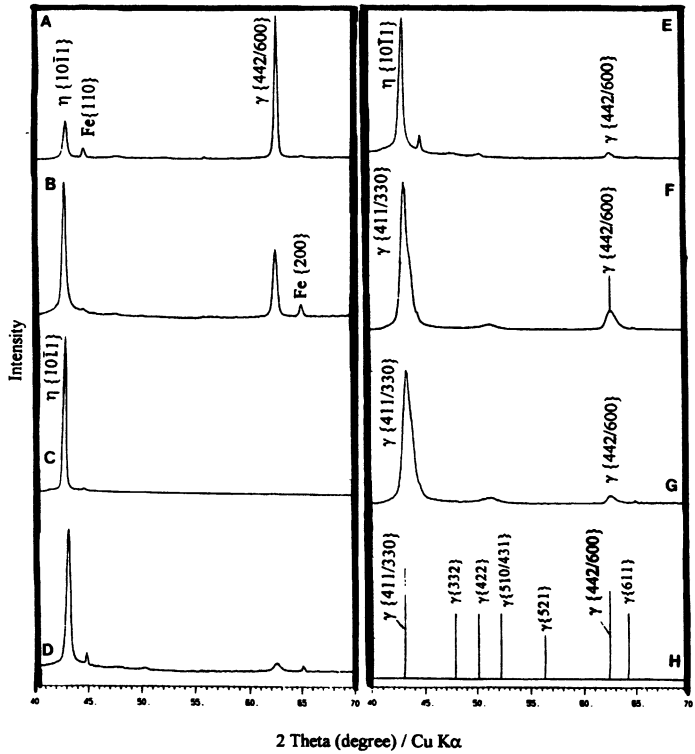

FIGURE 12 X-ray diffractometry of zinc–nickel electrodeposited coatings at various current density: (a) 50, (b) 100, (c) 200, (d) 300, (e) 500, (f) 900, (g) 1200 mA/cm^2, and (h) standard peak position of γ phase of zinc–nickel.

However, the intensity of γ peak becomes weaker than η peak. The coatings deposited at the current density range from 200 to 500 mA/cm^2 have the η $\{10\bar{1}0\}$ peak, while the intensity of γ peak is small. When the current density reaches 900–1200 mA/cm^2, the η peak completely disappears, while the coatings have peaks which represent the γ {411/330} as well as the γ {442/600} peaks. The intensity of the γ {411/330} peak is stronger than the γ {442/600} peak.

The Microstress of Zinc–Iron Coatings

This section describes the changes of the diffraction peak broadening on zinc–iron coatings with different current densities. The internal microstress on coatings are analyzed by measuring the FWHM of the X-ray peak. Figure 13 illustrates the change of the FWHM of the $\{20\bar{2}3\}$ peak with current density. The FWHM continuously increases with the increasing current density. This peak broadening indicates that the internal stress continuously increases as the deposition current density increases.

The FWHM of the $\{11\bar{2}2\}$ peak is plotted as a function of the coating thickness in Fig. 14. The thinnest coating is the most highly stressed. However, the stress drops significantly as the coating thickness increases

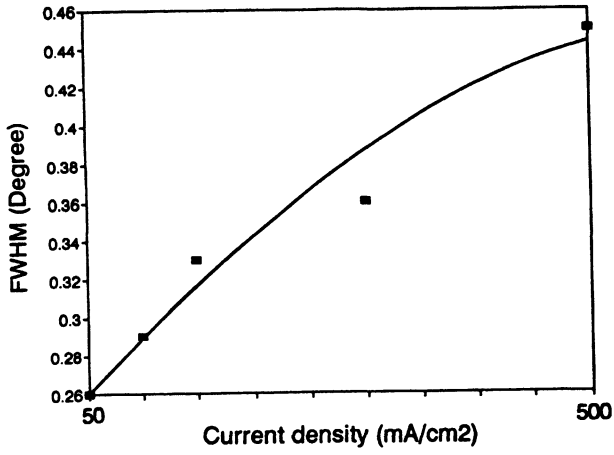

FIGURE 13 Change of FWHM of zinc–iron electrodeposited coatings with current density.

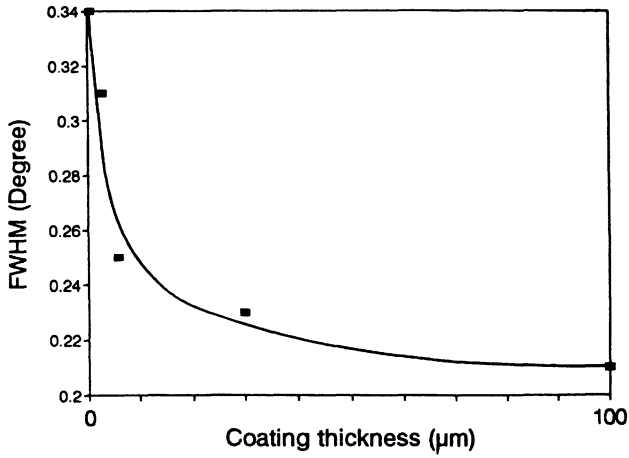

FIGURE 14 Change of FWHM of zinc–iron electrodeposited coatings with current thickness.

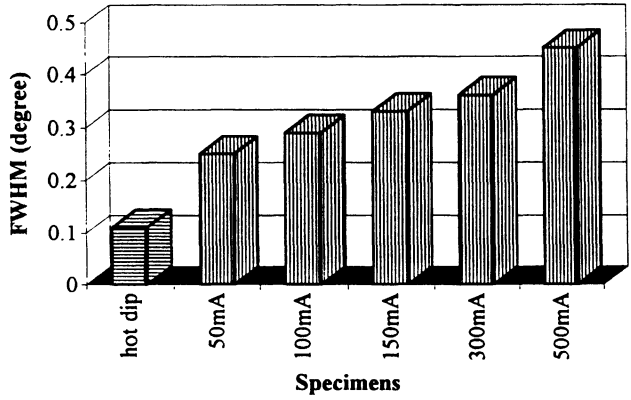

FIGURE 15 Difference of FWHM between hot-dip zinc–iron galvannealed coating and electrodeposited zinc–iron coatings obtained at various current densitites.

to 10 μm. A further increase in the coating thickness of up to 100 μm does not affect the stress significantly.

For the purpose of comparison, the FWHM of a commercially produced hot dip galvannealed coating is plotted along with those of electrodeposited coatings at various current densities in Fig. 15. The FWHM of hot-dip galvannealed coatings is smaller than all of the electrodeposited coatings. More specifically, the FWHM of a hot dip

galvannealed coating is less than half of the smallest FWHM of the electrodeposited coatings. This indicates that stored internal energy is released during the annealing process, thereby relieving the existing internal stress.

The Evolution of Coating Texture

The Texture of Zinc–Iron Coatings

Figure 16 shows the {0001} pole figures for the coatings deposited at different current densities. The coating deposited at 50 mA/cm^2 has two major texture components: the {0001} basal and the $\{10\bar{1}3\}$ pyramidal texture. The intensity of the basal pole texture is 33 times higher than the intensity from the random component. While the {0001} component shows a very sharp and strong fiber texture, the $\{10\bar{1}3\}$ component is affected by the steel substrate. The basal and the pyramidal texture components coexist until the deposition current density increases to 100 mA/cm^2.

As the applied current density increases to 200 mA/cm^2, the characteristics of zinc–iron coating textures change significantly. The basal texture component completely disappears, whereas the pyramidal texture component remains. It should be noted that this pyramidal component gradually transforms to the fiber texture component as the current density increases further. At the current density of 300 mA/cm^2, the coating texture transforms to a very weak fiber pyramidal texture component. This texture is widely dispersed, and is an incomplete fiber component with an intensity of 2.2 to the rolling direction, and an intensity of 1.2 to the transverse direction. Further increase in current density up to 500 mA/cm^2 leads to the $\{10\bar{1}3\}$ fiber texture. The pole figure of the coating deposited at 500 mA/cm^2 shows a widely dispersed fiber component with an intensity of 2.1 times higher than random.

The Texture of Zinc–Nickel Coatings

This section describes the evolution of texture during the electrodeposition of zinc–nickel coatings at different current densities. Figure 17 shows the pole figures of electrodeposited zinc–nickel coatings obtained in the current density range of 50–1200 mA/cm^2. It should be noted that the coatings with the γ phase have two

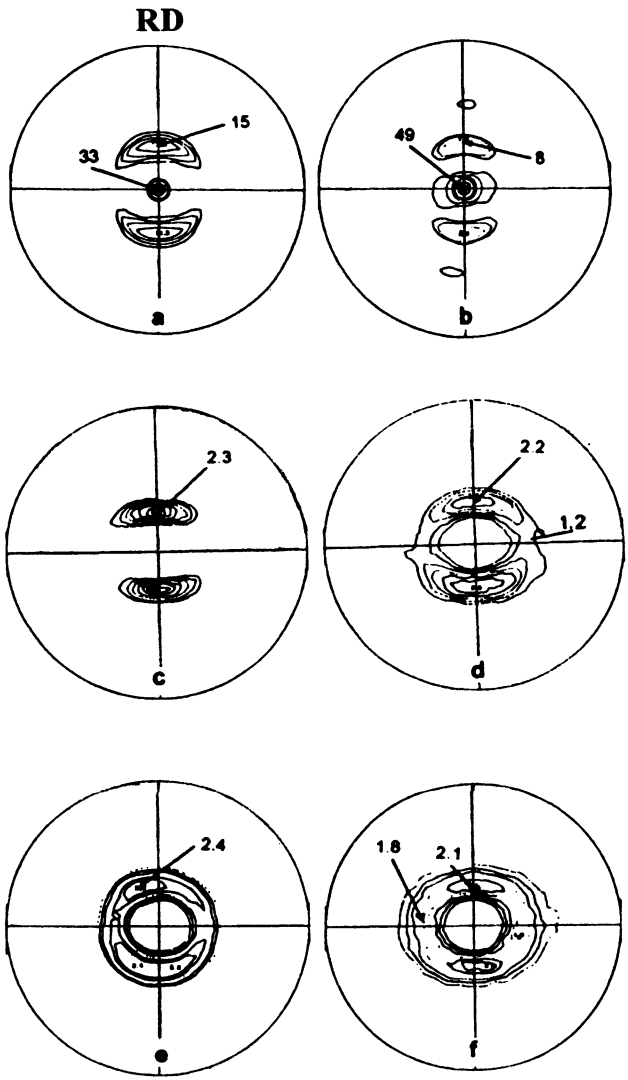

FIGURE 16 The {0001} pole figures of zinc–iron electrodeposited coatings deposited at different current density: (a) 50, (b) 100, (c) 200, (d) 300, (e) 400, (f) 500 mA/cm^2; the basal component completely disappears at 200 mA/cm^2 while the non-fiber pyramidal component gradually evolves to fiber at higher current density.

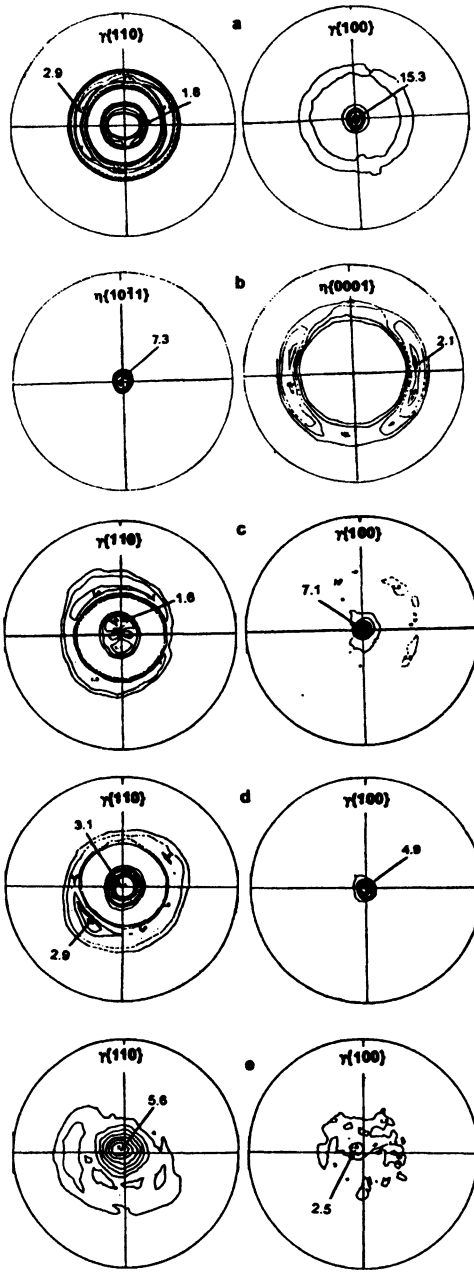

FIGURE 17 The pole figures of zinc–nickel electrodeposited coatings deposited at different current density: (a) 50, (b) 200, (c) 700, (d) 900, (e) 1200 mA/cm^2.

X-ray diffraction peak maxima at which two sets of {*hkl*} planes overlap. One is the peak at which {330} and {411} maxima overlap. The other is the peak maxima which consists of {600} and {442} reflections. In order to describe the texture, it is necessary to identify from which of the two planes the X-rays are diffracted. There is no direct method to separate the maxima from two different planes, because those planes have the same diffraction angle which satisfies Bragg's law. Therefore, the texture can only be identified by comparing the {*hkl*} interplanar angles with the pole locations in the pole figures. Two pole figures were measured from the 2θ positions of two peak maxima. For example, the pole figures of the coating deposited at 50 mA/cm^2 are shown in Fig. 17(a). The pole figure obtained from the {330/411} diffraction maxima shows two rings located at 20° and 45°. The other pole figure obtained from {600/442} peak shows the intensity maxima at the center of the pole figure. To identify whether the coating has {100} or {221} fiber texture, the interplanar angle between those planes are calculated, and subsequently compared with the maxima that are observed in the pole figure. The ring at 20° corresponds to the interplanar angle between {100} and {411}, while the ring at 45° corresponds to the interplanar angle between {100} and {110}. In the case of the {221}, however, the interplanar angles do not correspond to the ring positions. Therefore, it can be suggested that the coating has {100} fiber texture.

At a current density of 200 mA/cm^2 the {100} fiber texture completely disappears, whereas the {1011} fiber texture which characterizes the η phase becomes a main texture component (Fig. 17(b)). No significant change in texture is found when the current density increases up to 500 mA/cm^2. As the deposition current density increases further to 700 mA/cm^2, the γ phase dominates, and the {110} and the {100} textures are observed (Fig. 17(c)). The intensity maxima characterizing both textures are 1.6 and 7.1, respectively. The {110} texture is weak and plane orientations are widely dispersed within the range of 20°, while the {100} texture is strong and the maxima is well defined. A further increase in the current density range of 900–1200 mA/cm^2 causes continuous changes in the texture intensity (Fig. 17(d) and (e)). The intensity of the {110} texture, for instance, increases to 3.1 and then to 5.6, while the intensity of the {100} component decreases to 4.9 and then to 2.5.

DISCUSSIONS

The Evolution of Coating Morphology at Different Deposition Parameters

The Influence of Current Density

From the experimental results, it was demonstrated that the surface morphology of zinc–iron coatings changes from hexagonal platelets and ridges to triangular-based pyramidal grains, while the iron content in the deposit increases with increasing current density. Therefore, the comparison of coating morphology and alloy composition indicates that changing the current density is responsible not only for the evolution of coating morphology, but also for the change of alloy composition in the deposit.

The present results show that the percentage of a more noble metal (iron) in the deposit increases as the current density increases from 50 to 500 mA/cm^2. This phenomenon can be attributed to the anomalous codeposition behavior of alloy coatings (Brenner, 1963). At high applied current density, the zinc ion will be deposited preferentially at the initial state and subsequently, the electrolyte near the cathode surface is depleted of zinc ions. Since the metal deposition occurs only at the interface between the cathode and the electrolyte, where the migration of zinc ion is under diffusion control, the zinc content in the deposit should decrease as a consequence. Moreover, high current densities promote an increase of hydrogen evolution which results in a lack of agitation which subsequently develops the zinc depletion layer.

In the case of zinc–nickel coatings, the decrease of nickel content at the range of low current densities can be attributed to the normal type of codeposition, that is, the content of the more noble metal (nickel) decreases with increasing current density. A further increase in current density, eventually results in the anomalous codeposition in which the nickel content in the deposit increases significantly due to the high depletion in zinc ions at the cathode film.

The Influence of Coating Thickness

In this study, zinc–iron coatings exhibited an inhomogeneous alloy composition and morphology at different coating thicknesses. The

changes in the alloy composition of coatings can be explained by two phenomena proposed by Brenner (1963); (1) the nature of the initial cathode surface, and (2) the diffusion phenomenon. Brenner noted that cathode overpotential or current efficiency can influence the composition of electrodeposited alloys. Since the cathode surface of the substrate metal is immediately covered with a layer of the deposit, the next layer is less affected by the substrate, therefore allowing different morphologies to be formed in the thicker deposits. This discussion, however, is confined to a very thin layer, and thus is insufficient to explain the observation of the continuous decrease of iron content up to 100 μm, since the effects of the substrate would diminish as soon as the coating became a few layers thick, and consecutive layers would contact another layer of coating and not the substrate.

The diffusion phenomenon in the vicinity of the cathode surface will also affect the composition of the deposit. At the initial state of deposition, the concentration of more noble metal ions (iron) in the electrolyte adjacent to the cathode starts to decrease and eventually reaches a steady state in which the concentrations become constant. Since more noble metals preferentially deposit at the initial stage of the deposition, a thin deposit exhibits a higher concentration of noble metal than a thick deposit. The experimental results indicate that the concentration of the more noble metal (iron) is higher in the layers close to the substrate and gradually decreases as the coating thickness increases. There is other supportive evidence showing how thickness affects the alloy composition. In zinc–copper codeposition, Brenner (1963) reported that the initial deposit contains a higher percentage of noble metal (copper), and this percentage gradually decreases as thickness increases.

The morphological observation also suggests that the change of the cathode surface area can influence the alloy composition in the deposits. It was observed that the surface morphology of the coatings consists of pyramidal grains when the coating thickness is under 10 μm. A further increase in thickness, however, is associated with a rough surface morphology and subsequently increases the total cathode surface area. This fact causes the redistribution of current density on the cathode surface. During the electrodeposition, the applied current is kept constant. Thus, the real value of current density would decrease because of the surface area increase, as the coating thickness increases.

It should be noted that in these observations the alloy composition changes significantly in the range of thick coatings (10–100 μm), whereas only a small change was observed in the thin coatings (< 10 μm). This fact indicates that the thin coatings are more homogeneous and less rough than thick coatings. In its commercial application, zinc–iron coatings have a thickness of about 5–8 μm, and no significant change of alloy composition is found at this thickness range. It was also found that the coating obtained at high applied current density has a higher iron content than the coating deposited at low current density. The coating deposited at 500 mA/cm^2 with a thickness of 100 μm has the pyramidal morphology and about 8% of iron, whereas the coating deposited at 300 mA/cm^2 contains 0.6% iron in the deposit. This fact indicates that high applied current compensates for the current density drop caused by an increase of surface area in thick deposits.

PHASE COMPOSITION AND THE MICROSTRESS OF ALLOY COATINGS

The Phase Transformation of Zinc–Nickel Coatings

The present observation of X-ray diffraction patterns in Fig. 12 indicates that the zinc–nickel coatings have the $\eta + \gamma$ dual phase at the current density range of 50–100 mA/cm^2, and the coatings have the η single phase at the range of 200–500 mA/cm^2. This also indicates that the coatings have the γ single phase at the current density range of 900–1200 mA/cm^2. Therefore, the result indicates that the phase of zinc–nickel coatings transforms with changes in current density.

It was previously observed in results section above that the nickel content changes with current density changes. Obviously, the amount of nickel in the deposit determines the phase composition of the zinc–nickel alloy coatings. The phase transforms from η, through γ, to α with the increase of nickel content. It is reasonable, therefore, to compare the results of phase transformation with the previous observation of the change of nickel content. A good agreement is found between the phase composition and the nickel content in the deposit. The coatings of the η single phase have the lowest nickel content ranging from 13% to 15% at the current density range of 200–500 mA/cm^2. The coatings of

the $\eta + \gamma$ dual phase show an increase in nickel content to 17% at 50 mA/cm^2. The coatings of the γ single phase have the highest nickel content of up to 42% at the current density of 1200 mA/cm^2.

The present study demonstrated that the phase of zinc–nickel coatings transforms from the single η phase, through the dual $\gamma + \eta$ phase, to the γ phase, as the nickel percentage in the deposit increases. This dual phase has also been reported on by other studies on zinc–nickel coatings produced by pulse plating (Alfantazi *et al.*, 1994; Alfantazi, 1994). In the pulse plating cases, however, the dual phase exists at a low nickel content (8–12%). This differs from the present result obtained from DC plated coatings because the single η phase exists at a low nickel content, while the dual phase is formed only at a high nickel content ($\sim$ 17%). Different plating methods may be responsible for the existing difference. At low nickel contents, the η phase is the major phase. The evolution of a secondary γ phase, therefore, should be followed by the diminishing of the η phase. The evolution of the γ phase can be attributed to the effect of a local galvanic cell between two phases, which was argued by Kondo (1994). Kondo proposed that the formation of a local galvanic cell between the η and the γ phase during pulse current-off time might dissolve the η phase selectively and promote the formation of a secondary γ phase and consequently produce the $\gamma + \eta$ dual phase even at low nickel content. Other experimental results are in agreement with the present observations (Fountoulakis *et al.*, 1984). They reported that the dual $\gamma + \eta$ phase formed at low nickel contents ($\sim$ 8%) in the case of pulse plating, whereas only the single η phase was obtained in DC plated coatings.

It was demonstrated earlier that the morphology of zinc–nickel coatings evolves with a nickel content increase from the pyramidal grains, through the mixed morphology of pyramids and tiny particles and finally to the "cauliflower-like" structure. Similar findings are reported by other researchers (Kondo, 1994; Alfantazi *et al.*, 1994; Alfantazi, 1994). Alfantazi *et al.* (1994) observed that the morphology of zinc–nickel coatings change from hexagonal platelets to nodular and eventually to "cauliflower-like" structures when the nickel content increases. Kondo (1994) found that the morphological characteristics of the $\eta + \gamma$ dual phase is tiny submicron size granules, which represent the γ phase dispersed among the pyramidal grains of the η phase. Those observations are in agreement with the present study.

The Microstress of Zinc–Iron Coatings

The present results in Figs. 13 and 14 implies that internal stress increases with an increase of the current density and also that stress is high for thin coatings. The increase of stress with the current density can be attributed to the influence of current density upon the coating microstructure. High current densities induce a high nucleation rate. A high nucleation rate causes the deposit to have a high dislocation density and lattice distortion because ad-atoms on the cathode surface do not have enough time to move to the step or kink sites. This subsequently leads to the deposit to a state of high internal stress. The high microstress in the thin coatings is attributed to the strong influence of the substrate.

It was found that the zinc–iron coatings exhibit significant compositional change with current density and coating thickness. Since the peak broadening analysis was conducted on zinc–iron coatings, it is reasonable to extend the discussion to the influence of alloy composition upon the microstress of the coatings. The coatings with a high iron content have a high level of microstress. It appears that the incorporation of iron atoms and zinc atoms into the deposition site induces lattice distortion because of the difference in atom size, and therefore causes internal stress. This observation is in good agreement with another experimental finding which described an increase of microstress with an increase of alloy content in the deposit (Armyanov and Sotirova-Chakarova, 1993).

THE TEXTURE TRANSFORMATION OF ZINC ALLOY COATINGS

In the present study, it was found that the texture of zinc–iron coatings evolves from the {0001} basal fiber and the $\{10\bar{1}3\}$ pyramidal non-fiber component to the pyramidal fiber texture with a current density increase. This result is similar to the texture evolution of zinc coatings. The texture of zinc–iron coatings at low current densities in the range between 50 and 100 mA/cm^2 is quite similar to that obtained in pure zinc coatings (Park and Spunar, 1997). The basal fiber and the pyramidal non-fiber texture components are also observed there. This is attributed to the fact that at low current density, the iron content in the deposit is less than 3%

and thus the texture characteristics of the zinc–iron coating is close to that of zinc coatings.

The mechanism of texture evolution developed by different current densities was previously discussed by Park and Szpunar (1997). The correlation of the texture and morphology of coatings was also demonstrated at different deposition parameters. When the deposition parameters change, the iron content of zinc–iron coatings also changes. This compositional change is directly responsible for the characteristics of coating morphology which, in turn, lead to texture evolution. Therefore, it is necessary to discuss whether the iron content in zinc–iron coatings is related to the texture. The previous result of the EPMA (Fig. 3) showed that the iron content abruptly jumped from less than 2–10% as the current density increased from 50 to 300 mA/cm^2, while the present observation found a major transformation of texture at the same current density range. This fact indicates that there is correlation between the alloy content and the coating texture. With an increase of iron content in the deposit, the coating texture is transformed from the {0001} fiber and the $\{10\bar{1}3\}$ non-fiber component to the $\{10\bar{1}3\}$, fiber texture.

In the case of zinc–nickel coatings, it was found that the texture transforms at different current densities. It is known as well that the current density is directly responsible for changing the nickel content of the deposit, the texture changes can then be linked to the change of nickel content. Since the coatings have a low nickel content of 13–15% in the current density range of 200–500 mA/cm^2, the η phase is formed and the corresponding texture has only a pyramidal component. It is interesting to compare this result to the exclusive formation of the pyramidal texture in zinc–iron coatings of similar alloy composition. This observed similarity suggests that in both cases, the pyramidal component dominates when the alloying element content increases in this range. The coatings have a high nickel content of more than 21% in the current density range of 700–1200 mA/cm^2. In this range, the γ phase is formed and the corresponding texture intensity varies with the nickel content.

CONCLUSIONS

The characteristics of microstructure are demonstrated at various current densities during the deposition of zinc–iron and zinc–nickel

coatings. This work suggests that the evolution of texture during alloy codeposition is closely related to the morphological characteristics and the change of alloy and phase composition of the deposits.

(1) Investigation of zinc–iron coatings demonstrates that the texture evolves from the basal fiber and non-fiber pyramidal components to the pyramidal fiber texture when the current density increases from 50 to 500 mA/cm^2. Other parameters are kept constant (pH: 3.8 and coating thickness: 5 μm).
(2) The iron content in the zinc–iron coatings increases with the current density increase, whereas the c/a ratio decreases.
(3) The morphology of zinc–iron and zinc coatings is strongly correlated with texture. The morphology of hexagonal ridges represents the $\{10\bar{1}3\}$ non-fiber texture. The morphology of flat hexagonal platelets represents the {0001} fiber texture. The $\{10\bar{1}X\}$ fibre texture corresponds to the morphology of triangular pyramids which represents a hexagonal columnar crystal tilted from the substrate surface; one wall of the pyramid represents the {0001} basal plane, while the other two walls represent the $\{10\bar{1}0\}$ prismatic planes.
(4) The morphology of zinc–nickel coatings changes with the current density range of 50–1200 mA/cm^2. Other deposition parameters are kept constant (pH: 2.3 and coating thickness: 15 μm). The morphology of pyramidal grains and tiny particles transforms to the pyramidal grains, and finally to the "cauliflower-like" structure. This morphological transformation is associated with compositional changes from 13% to 42% Ni, and changes in phase composition. The phase composition of coatings changes from the η single phase, to $\gamma+\eta$ dual phase and is then transformed to the γ single phase.

References

Alfantazi, A.M., EI-Sherik, A.M. and Erb, U. (1994). *Scripta Metallurgica et Materialia*, **30**, 1245.

Alfantazi, A.M. (1994). A study on the synthesis, characterization and properties of pulseplated ultrafine-grained Zn–Ni alloy coatings, Ph.D. thesis, Queen's University, Kingston, Ontario.

Armyanov, S. and Sotirova-Chakarova, G. (1993). *Metal Finishing*, March, p. 42.

Brenner, A. (1963). *Electrodeposition of Alloys*, Vols. I and II, Academic Press. New York.

Chen, Y.L. and Snyder, D.D. (1990). *Proc. TMS Symposium on Zinc-Based Steel Coating Systems* (Krauss, G. and Matlock, D.K., Eds.), Detroit, Michigan, October 7–11, p. 95.

Fountoulakis, S.G., Steinbicker, R.N. and Fisher, T.W. (1984). *Proc. AES 4th Continuous Strip Plating Symposium*, Chicago, Illinois, May 1–3.

Irie, T. (1990). *Proc. TMS Symposium on Zinc-Based Steel Coating Systems* (Krauss, G. and Matlock, D.K. Eds.), Detroit, Michigan, October 7–11, p. 143.

Johnson, W.R. and Vrable, J.B. (1984). SAE Paper, no. 840213.

Kondo, K. (1994). Morphology and microstructure of electrodeposited zinc–iron and zinc–nickel binary alloys: A basic study on surface treatment of steel sheets used for automobile body, Ph.D. thesis, Kyoto University, Kyoto, Japan.

Lin, Y. (1992). Microstructure of zinc-based coatings on steel sheets, Ph.D. thesis, Northwestern University, Evanston, Illinois.

Lowenheim, F.A. (1978). *Electroplating*, McGraw-Hill Book Co., New York.

Park, H. and Szpunar, J.A. (1998). The role of texture and morphology in optimizing the corrosion resistance. *Corrosion Sci.*, **40**, 525.

Shima, Y., Terasaka, M., Nakaoka, K., Hara, T. and Honma, T. (1986). *Tetsu-to-Hagan*, **8**, 954.